Nanoscale

PAPER

View Article Online
View Journal | View Issue

Cite this: *Nanoscale*, 2014, **6**, 5432

Phase transitions of a water overlayer on charged graphene: from electromelting to electrofreezing†

Xueyan Zhu, Quanzi Yuan and Ya-Pu Zhao*

Received 12th December 2013
Accepted 3rd March 2014

DOI: 10.1039/c3nr06596k

www.rsc.org/nanoscale

We show by using molecular dynamics simulations that a water overlayer on charged graphene experiences first-order ice-to-liquid (electromelting), and then liquid-to-ice (electrofreezing) phase transitions with the increase of the charge value. Corresponding to the ice–liquid–ice transition, the variations of the order parameters indicate an order–disorder–order transition. The key to this novel phenomenon is the surface charge induced change of the orientations of water dipoles, which leads to the change of the water–water interactions from being attractive to repulsive at a critical charge value q_c. To further uncover how the orientations of water dipoles influence the interaction strength between water molecules, a theoretical model considering both the Coulomb and van der Waals interactions is established. The results show that with the increase of the charge value, the interaction strength between water molecules decreases below q_c, then increases above q_c. These two inverse processes lead to electromelting and electrofreezing, respectively. Combining this model with the Eyring equation, the diffusion coefficient is obtained, the variation of which is in qualitative agreement with the simulation results. Our findings not only expand our knowledge of the graphene–water interface, but related analyses could also help recognize the controversial role of the surface charge or electric field in promoting phase transitions of water.

Introduction

The properties of water adsorption on solid surfaces are fundamental to chemical and biological processes.[1,2] Particularly, due to the confinement of the solid surface, the possibility of freezing adsorbed water at room temperature has attracted considerable interest in recent years.[3–6] Graphene is in this respect of particular interest as a solid surface because unexpected phenomena have always been found when graphene comes into contact with water.[7–11] For example, Nair *et al.*[8] found that graphene is impermeable to everything but water, which is due to the fast transport of an ordered water film through graphene capillaries. Feng *et al.*[9] reported that epitaxial graphene with line defects can only be attacked by water from the environment, which splits the graphene film into numerous fragments, followed by water intercalation under the graphene. Recently, the ice-like structure on graphite has been imaged at room temperature through atomic force microscopy.[4,5] A hexagonal structure with a 0.45 ± 0.04 nm periodicity was observed. Although much progress has been made, the application of graphene in electronic devices deserves further investigation of water adsorption on charged graphene, which has not been reported to the best of our knowledge.

A two-dimensional (2D) water film would form when water adsorbs on graphene. Similar to bulk water, variations of external conditions can induce phase transitions of the 2D water film, which is of particular interest,[12–14] because phase transitions influence both the properties[15–17] of the adsorbed water and the solid surface. Fundamentally, phase transitions are largely determined by the interactions between molecules. The dipolar nature of water makes the water–water interactions easily disturbed by external charges or electric fields, which was reported to promote freezing of both the bulk and adsorbed water, so-called electrofreezing.[18–22] The reverse process, electromelting,[23] has also been reported recently. This raises the controversial role of the electric field in promoting phase transitions of water and the related mechanisms become confusing.

In this paper, employing molecular dynamics (MD) simulations, for the first time we show that the adsorbed water on charged graphene experiences phase transitions from electromelting to electrofreezing. This novel phenomenon is attributed to the change of the water–water interactions from being attractive to repulsive at a critical charge value q_c. With the increase of the charge value, the strength of the attractive water–water interactions decreases below q_c, while that of the repulsive water–water interactions increases above q_c. These two inverse processes lead to electromelting and electrofreezing,

State Key Laboratory of Nonlinear Mechanics, Institute of Mechanics, Chinese Academy of Sciences, Beijing 100190, People's Republic of China. E-mail: yzhao@imech.ac.cn

† Electronic supplementary information (ESI) available. See DOI: 10.1039/c3nr06596k

respectively. To further investigate the dynamic properties of the adsorbed water, the transition state theory is extended by including both water–water interactions and water–graphene interactions in the Eyring equation. The theory and the simulations qualitatively agree well with the diffusion coefficient, the variation of which further confirms the ice–liquid–ice transition. Our findings should shed new light on the surface charge induced phase transitions and the related analyses could help uncover the mechanisms of electromelting and electrofreezing.

Models and methods

MD simulations implemented in LAMMPS[24] are carried out in the NVT ensemble with a timestep of 1 fs. The Nose–Hoover thermostat is used to keep the temperature of the system at 300 K, and the temperature is relaxed in the timespan of roughly 10 fs. The graphene surface has dimensions of 98.40 × 93.72 Å^2 parallel to the x–y plane. Periodic boundary conditions are applied along directions x and y. Carbon atoms are fixed during the whole process. The van der Waals interactions between water atoms and carbon atoms are modeled by the Lennard-Jones (LJ) potential with $\varepsilon_{O\text{–}C} = 0.15$ kcal mol^{-1}, $\sigma_{O\text{–}C} = 3.39$ Å and $\varepsilon_{H\text{–}C} = 0.00$ kcal mol^{-1}, $\sigma_{H\text{–}C} = 0.00$ Å (these parameters are tested by comparing with density functional theory simulations in ESI 8 of ref. 25).

An extended single point charge (SPC/E) water model[26] is used. Although the SPC/E water model is simple compared with TIP4P and TIP5P and even fails to reproduce the phase diagram,[27] the physical properties of water at room temperature predicted by this water model are closer to the experimental values.[28–31] In addition, the structure of the water overlayer on graphene predicted by SPC/E is closer to the experimental results than that by TIP4P (see ESI 7†).

First, a thin water film extracted from bulk water is placed on uncharged graphene. The number of water molecules (1320) is chosen so as to ensure that approximately a monolayer of water forms on the uncharged graphene after equilibration. Then, the carbon atoms are charged with $q = 0.00$–0.18 e gradually (the case of $q = -0.00$–0.18 e is shown in ESI 5†). The determination and choice of the upper bound for the charge value are discussed in ESI 6.† The electric field is generated by the surface charge and outwards the graphene surface. Under the electric field, not only the structure of the water film changes, but the number of water layers also increases. In this paper, we focus on the lateral structure change and phase transitions of the first layer water. The transverse change is discussed in ESI 1.† The adsorption process on a certain charged graphene surface is simulated until the free energy of the whole system converges around a fixed value. The total simulation time ranges between 5 and 12 ns depending on q. After equilibration, an additional 2 ns is used for data acquisition.

Results and discussion

To examine how the structure of the first layer water changes in the process of charging graphene, we plot the evolution of the lateral oxygen–oxygen radial distribution function (RDF) with respect to q (Fig. 1). For $q = 0.00$–0.06 e, the RDF exhibits long-range order, indicating an ordered crystalline phase. As visualized in Fig. 2(a), this ice structure is hexagonal, which is in agreement with the experimental results.[4] When q increases to 0.07 e, the behaviour of the RDF changes abruptly as shown in Fig. 1(b). The RDF of $q = 0.07$ e consists of a pre-peak followed by rapidly decaying peaks and the eventual approach to unity, which is characteristic of short-range order and corresponds to the liquid state (Fig. 2(b)). Therefore, the ice-to-liquid phase transition occurs at q_{c1} between $q = 0.06$ e and $q = 0.07$ e. The abrupt change suggests a first-order (discontinuous) transition. For $q = 0.07$–0.12 e (Fig. 1(b)), the first peak of the RDF ($r = 2.75$ Å) becomes lower with the increase of q, indicating the evolution to a more disordered state. Simultaneously, the second peak localized at $r = 3.75$ Å increases. When q increases to 0.12 e, the second peak outstrips the first peak, indicating the increase of the distance between water molecules. Then, when q is varied across q_{c2} between $q = 0.12$ e and $q = 0.13$ e, the character of the RDF abruptly changes from disordered to ordered (Fig. 1(c)), reflecting a discontinuous liquid-to-ice phase transition. In this case, the ice structure is also hexagonal (Fig. 2(c)). A similar surface charge induced disorder-to-order transition was imaged by scanning tunnelling microscopy in an organic monolayer.[32] For $q = 0.13$–0.18 e, the RDF experiences almost no change, except the increase of the peaks, indicating the evolution of the water overlayer to a more ordered state. Therefore, the RDF results suggest an ice–liquid–ice transition of the water overlayer, which is also a process of the order–disorder–order transition.

Note that the ice structure before the first transition point q_{c1} (denoted by ice I, Fig. 2(a)) is different from that after the second transition point q_{c2} (denoted by ice II, Fig. 2(c)), though they are

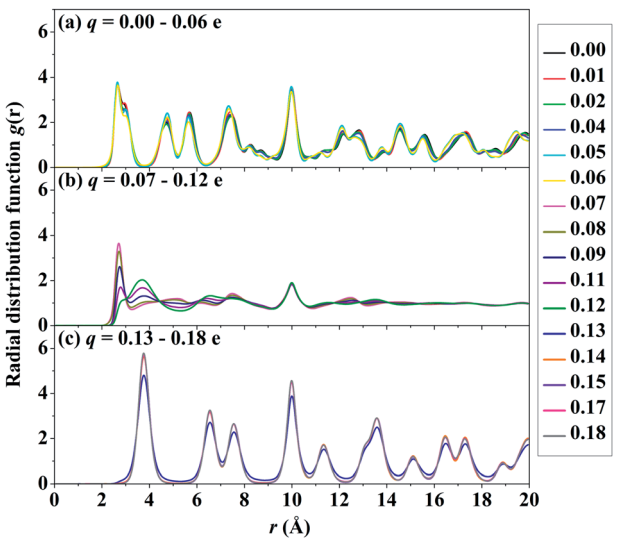

Fig. 1 Evolution of lateral oxygen–oxygen RDF with respect to charge values q. (a) The RDF exhibits characteristic features of solids for $q \leq 0.06$ e. (b) When q is varied across q_{c1} between 0.06 e and 0.07 e, the RDF changes abruptly, indicating a first-order ice-to-liquid transition. (c) The liquid-to-ice transition occurs at q_{c2} between 0.12 e and 0.13 e, as indicated by the abrupt change of the RDF's character.

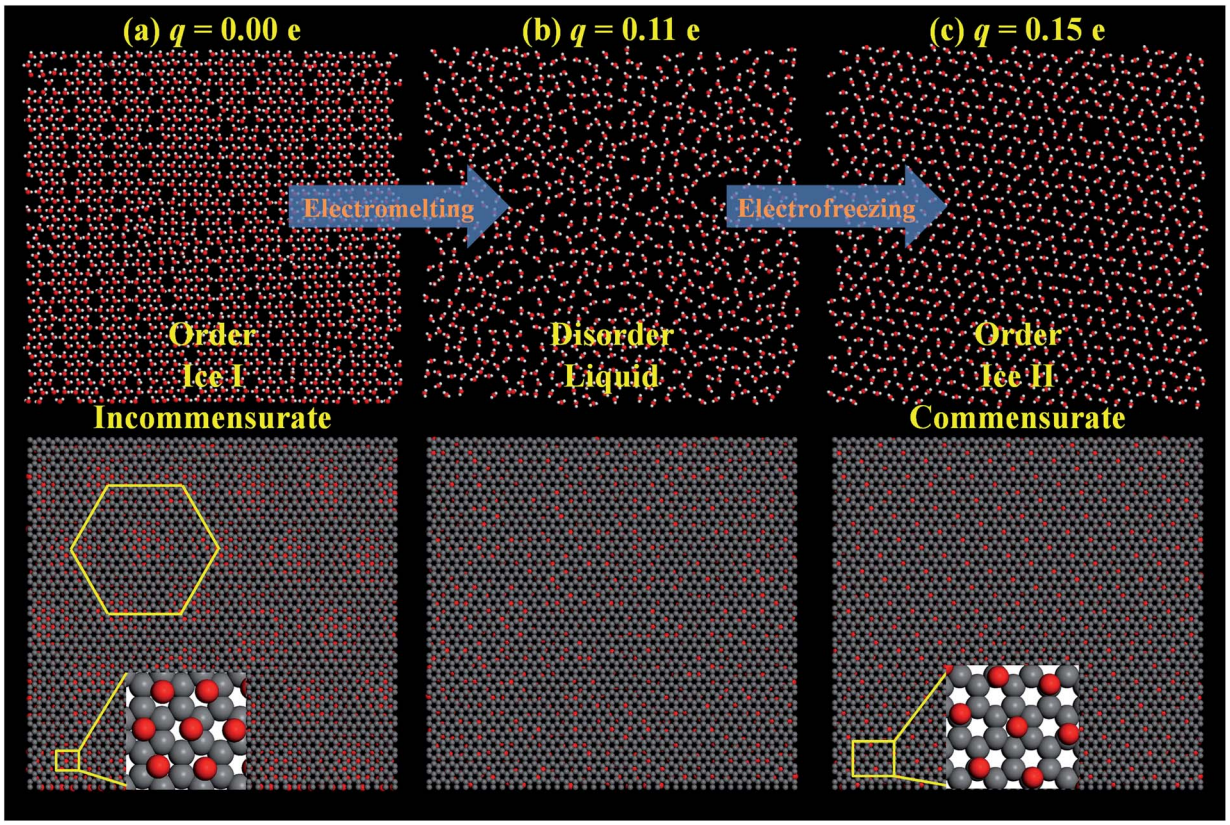

Fig. 2 Snapshots of the first layer water on graphene. Red, white and grey atoms represent oxygen, hydrogen and carbon atoms, respectively. The upper figures show the water monolayer without the display of graphene, while the lower figures show the distribution of oxygen atoms with the display of graphene. (a) $q = 0.00$ e. Water molecules arrange in a hexagonal structure which is incommensurate with graphene. The moiré pattern is visible in the lower figure, the unit cell of which is also hexagonal and plotted by yellow lines. (b) $q = 0.11$ e. Water monolayer exhibits a liquid state, the structure of which is disordered. (c) $q = 0.15$ e. The ice structure in this case is also hexagonal, but commensurate with graphene.

all hexagonal. From the first peaks of the RDFs, the first neighbours (lattice constant) of ice I and ice II are obtained to be $a_{\mathrm{I}} = 2.65$ Å and $a_{\mathrm{II}} = 3.75$ Å, respectively. Using Wood's notation, ice I can be denoted by $c(1.87 \times 1.87)R30^{\circ}$ with vacancies, which is incommensurate with graphene, while ice II $c(2.64 \times 2.64)R19.12^{\circ}$ commensurate with graphene. Due to the incommensurateness between ice I and graphene, the moiré pattern with a hexagonal structure is visible (see the bottom figure in Fig. 2(a)). The moiré motifs have attracted a considerable amount of interest in both theoretical investigations[33,34] and potential applications.[35,36] For example, the moiré pattern of a graphene–iridium sandwich is found to provide patterned adsorption positions for atomic hydrogen in the application of the bandgap opening of graphene.[35] Here, the potential applications of the moiré pattern of the graphene–water sandwich should be an interesting issue for further exploration.

What is the nature of the ice–liquid–ice transition, and why is ice I incommensurate, while ice II commensurate with graphene? To address these questions, the water–water interaction energy $E_{\mathrm{w-w}}$ and water–graphene interaction energy $E_{\mathrm{w-g}}$ are calculated as shown in Fig. 3. When $q < q_{\mathrm{c}}$, $E_{\mathrm{w-w}}$ is negative, indicating attractive water–water interactions. For $q = 0.00$ e, water molecules attract one another to form a 2D hydrogen bond (H bond) network, *i.e.*, ice I. Ice I cannot be registered on graphene (incommensurateness) due to the stronger water–water interactions ($E_{\mathrm{w-w}} = -14.14$ kcal mol^{-1}) compared with water–graphene interactions ($E_{\mathrm{w-g}} = -1.85$ kcal mol^{-1}). With the increase of q, $|E_{\mathrm{w-w}}|$ decreases, indicating the decreasing

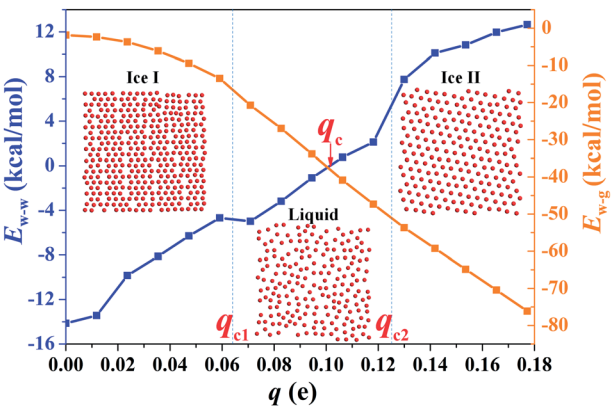

Fig. 3 The variation of water–water interaction energy $E_{\mathrm{w-w}}$ (blue curve) and water–graphene interaction energy $E_{\mathrm{w-g}}$ (orange curve) with respect to q, respectively. The inset shows the structure of the water monolayer by displaying oxygen atoms only. The water–water interaction is attractive below q_{c}, while repulsive above q_{c}.

strength of the attractive water–water interactions. As q is varied across q_{c1}, we find a drop in E_{w-w}, which is consistent with the first-order phase transition between ice and liquid at q_{c1}. Above q_{c1}, $|E_{w-w}|$ further decreases, leading to the evolution of the liquid phase to a more disordered state. When $q > q_c$, E_{w-w} becomes positive. That is to say, the properties of water–water interactions become repulsive, which is responsible for the increase of the distance between water molecules. A further increase of q is accompanied by the increase of $|E_{w-w}|$, suggesting the increasing strength of the repulsive water–water interactions. At q_{c2}, a sudden increase of $|E_{w-w}|$ occurs, indicating the freezing of the liquid phase and the formation of ice II (liquid–ice transition). We noticed that $|E_{w-g}|$ (53.68–76.12 kcal mol^{-1}) is much larger than $|E_{w-w}|$ (7.75–12.65 kcal mol^{-1}) when $q > q_{c2}$. This reflects stronger water–graphene interactions compared with water–water interactions, which results in the commensurateness between ice II and graphene. From the above discussions, we note that the mechanisms for the formation of ice I and ice II are distinctly different: ice I is aggregated by the strong attractive water–water interactions, while ice II by the strong repulsive water–water interactions.

We further probe the symmetrical properties of the water overlayer by computing the order parameters of both orientation and position in Fig. 4. The orientational order parameter, S, is defined as:

$$S = \frac{1}{2}\langle 3\cos^2\phi - 1\rangle \quad (1)$$

where ϕ is the angle between the surface normal and the dipole vector of water and the brackets represent the average over all the water molecules and a long-time range. If all the water molecules are parallel to the graphene surface, $S = -0.5$. If the orientations of water molecules are totally disordered, $S = 0$. If all the water molecules are perpendicular to the graphene surface, $S = 1.0$. Thus, the continuous increase of S from approximately −0.5 to 1.0 with respect to q (Fig. 4(a)) suggests that the water dipoles gradually change from being almost all parallel to the surface to almost all perpendicular to the surface. And the orientation of water dipoles experiences an order–disorder–order transition in the course of charging graphene. When the orientations of water dipoles are almost parallel to the graphene surface, neighbouring water molecules are linked *via* the negative oxygen end and the positive hydrogen end, which leads to the attractive water–water interactions as shown in Fig. 3. After adding positive charges to the graphene, the graphene attracts the oxygen atoms of water molecules, while repels the hydrogen atoms. This results in perpendicular water orientations. In this case, neighbouring water molecules repel one another due to the side-by-side arrangement of the dipoles, which induces the repulsive water–water interactions and explains the energy profile in Fig. 3.

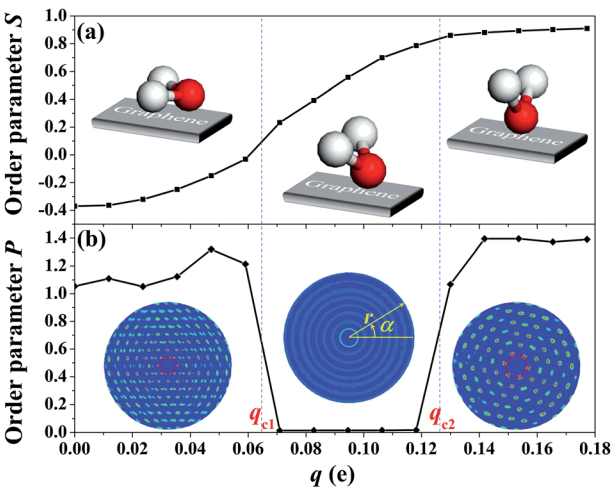

Fig. 4 The (a) orientational order parameter S and (b) positional order parameter P *vs.* the charge value q. The inset of (a) shows the schematic diagram of how the orientation of the water dipole changes in the course of charging graphene. The inset of (b) shows the ARDF, in which the density gradually decreases from red to blue.

To define the positional order parameter, we introduce the concept of the angle-dependent radial distribution function (ARDF) $f(r, \alpha)$, which describes how the normalized density varies as a function of the distance r from a reference atom and the angle α from a reference orientation. The ARDF reflects the rotational symmetry. ARDF $f(r, \alpha)$ that is independent of α indicates the highest rotational symmetry (isotropy), while the ARDF dependent on α indicates the broken symmetry (anisotropy). Based on the ARDF, the positional order parameter, P, is defined as:

$$P = \frac{\int_0^{2\pi}\int_0^{R} |f(r,\alpha) - \overline{f}(r)|\mathrm{d}r\mathrm{d}\alpha}{2\pi R} \quad (2)$$

where $\overline{f}(r) = \int_0^{2\pi} f(r,\alpha)\mathrm{d}\alpha/(2\pi)$ is the average of $f(r, \alpha)$ over α from 0 to 2π and $R = 20$ Å is the cutoff. Thus, the highest rotational symmetry corresponds to $P = 0$, while the broken symmetry $P \neq 0$. As shown in Fig. 4(b), $P \neq 0$ for $q = 0.00$–0.06 e, $P = 0$ for $q = 0.07$–0.12 e, and $P \neq 0$ for $q = 0.13$–0.18 e. This indicates that the water overlayer experiences an anisotropy–isotropy–anisotropy phase transition (inset of Fig. 4(b)) as q increases, which corresponds to the ice–liquid–ice transition. And the abrupt changes at the phase transition points q_{c1} and q_{c2} suggest the first-order transitions. Therefore, the ice–liquid–ice transition is accompanied by the change of the symmetrical properties of the water overlayer.

From the above discussions, we have known that the orientations of water dipoles change in response to the charging of graphene atoms. But, how do the orientations of water dipoles influence the water–water interactions? For simplicity, we examine the interaction energy between two water molecules (ESI 2† for details).

$$V \approx -\frac{Cu^2}{r^3}(2\cos\theta_1\cos\theta_2 - \sin\theta_1\sin\theta_2\cos\varphi) + 4\varepsilon_{O-O}\left(\frac{\sigma_{O-O}}{r}\right)^{12} \quad (3)$$

where C is the Coulomb's constant, u is the dipole moment of a water molecule, r is the distance between the centers of the dipoles, θ_1 and θ_2 are the angles between the dipole vectors and the vector connecting the two dipoles, φ is the dihedral angle

formed by the two dipole vectors and the connection vector, and ε_{O-O} and σ_{O-O} are the LJ parameters for oxygen atoms. Considering only the first-order approximation, the energy function V is expanded in a Taylor series around $r = a_0$ ($\partial V/\partial r|_{r=a_0} = 0$):

$$V - V(a_0) = \frac{1}{2}g(r-a_0)^2 + O(r-a_0)^3$$
$$g = \frac{27Cu^2}{82^{2/9}}\left(\frac{Cu^2}{\varepsilon_{O-O}\sigma_{O-O}^{12}}\right)^{5/9}(2\cos\theta_1\cos\theta_2 - \sin\theta_1\sin\theta_2\cos\varphi)^{14/9} \quad (4)$$

where g is the effective elastic constant (the constitutive parameter of the water overlayer) depending on the orientations of water dipoles. Through statistics of the orientations of water dipoles from MD results, we obtain the variation of g with respect to q as shown in Fig. 5(a). As q increases, g decreases below q_c; then increases above q_c. This is in agreement with the variation of $|E_{w-w}|$ (Fig. 3), which reflects the interaction strength between water molecules.

We further explore the dynamical properties by calculating the lateral diffusion coefficient of the first layer water. According to the Eyring equation, the diffusion coefficient is expressed by:

$$D = D_0\exp\left(-\frac{\Delta G_m}{k_BT}\right) = \frac{1}{4}\frac{k_BT}{h}a_s^2\exp\left(-\frac{\Delta G_m}{k_BT}\right) \quad (5)$$

where ΔG_m is the energy barrier, k_B is the Boltzmann constant, h is the Planck constant, T is the temperature and a_s is the distance between adsorption sites ($a_s = 2.46$ Å for graphene). In the above equation, $k_BT/h \sim 10^{13}$ s^{-1} is the fundamental frequency, which represents the mobility of the molecules activated by thermal energy. The motion of water molecules on the graphene surface is hindered not only by the viscous interactions between neighbouring water molecules, but also by water–graphene interactions. So the energy barrier $\Delta G_m = \Delta G_v + \varepsilon_s$, where ΔG_v is the contribution from viscosity and ε_s is the depth of the potential surface for water–graphene interactions (orange line in Fig. 5(a)). According to Eyring's theory,[37] the relationship between ΔG_v and viscosity η is $\Delta G_v = k_BT\ln(\eta v_L/h)$, where v_L is the volume of the unit of flow. The viscosity η is determined by the water–water interactions, and thus can be related to the elastic constant g by $\eta \sim \tau E \sim \tau g/l_z$,[38] where τ is the Maxwellian relaxation time (see ESI 3†), E is the elastic modulus and l_z is the size of the water overlayer along the z direction. Therefore, we can obtain D directly from g and ε_s through

$$D = \frac{1}{4}\frac{a_s^2}{\tau}\frac{k_BT}{gv_L/l_z}\exp\left(-\frac{\varepsilon_s}{k_BT}\right) = \frac{1}{4}\frac{a_s^2}{\tau}\frac{k_BT}{gs_L}\exp\left(-\frac{\varepsilon_s}{k_BT}\right) \quad (6)$$

in which $s_L \approx 9$ Å^2 is the area occupied by a water molecule in the water overlayer. Eqn (6) contains two non-dimensional numbers, $k_BT/(gs_L)$ and k_BT/ε_s, which represent the competition between the thermal energy and the energy dissipation from viscous interactions and water–graphene interactions, respectively. As shown in Fig. 5(b), when q approaches q_c, $k_BT/(gs_L)$ and k_BT/ε_s both approach unity, which is the critical point for the transition from electromelting to electrofreezing.

In addition, D can also be calculated by using the Einstein equation through statistics of the mean square displacement from MD simulations (see ESI 4† for details). As shown in Fig. 5(c), theoretical results agree qualitatively with MD results. For q = 0.00–0.06 e, D is in the range of 10^{-12}–10^{-10} m^2 s^{-1}, indicating the solid phase (ice I). At q_{c1}, the water film transforms to a liquid phase as indicated by the abrupt increase of D to the order of 10^{-9} m^2 s^{-1}. When q is increased to q_{c2}, D decreased to 10^{-12}–10^{-11} m^2 s^{-1} abruptly, indicating the freezing of the liquid phase and formation of ice II. Therefore, the diffusion coefficient provides further evidence for the ice–liquid–ice transition in the course of charging graphene.

We would like to compare our results with previous investigations on electromelting and electrofreezing. Recently, Guo *et al.*[23] reported melting of confined water between parallel plates under the electric field with a magnitude of 5 V nm^{-1}. Then, the liquid water freezes when the electric field intensity increases to 50 V nm^{-1}. In this paper, we investigate phase transitions of the water overlayer on an open surface of charged graphene. If the surface charge is converted to the magnitude of the electric field E, electromelting occurs at $E = 0.6$ V nm^{-1}. Then, electrofreezing occurs at E = 1.1 V nm^{-1}. The critical electric field intensity for electromelting and electrofreezing in our work is one order smaller than that reported by Guo *et al.* Previous studies also found that the critical electric field intensity for electrofreezing of bulk water[19,20] is typically one order (~1 V nm^{-1}) smaller than that for confined water[18,21] (~10 V nm^{-1}). These phenomena indicate that the confinement effect may hinder the phase transitions of water, which is of interest for further investigations.

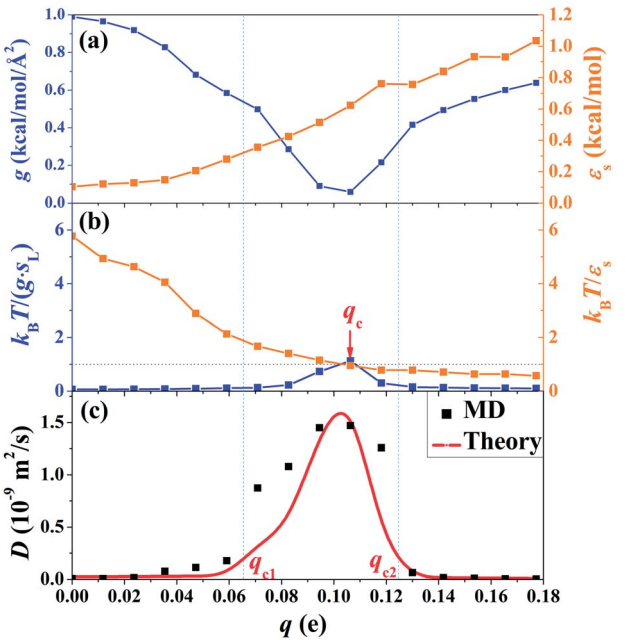

Fig. 5 (a) The variation of the effective elastic constant g for water–water interactions (blue curve) and the depth of the potential surface ε_s for water–graphene interactions (orange curve) with respect to q, respectively. (b) The variation of the non-dimensional numbers $k_BT/(gs_L)$ and k_BT/ε_s with respect to q, respectively. (c) Diffusion coefficient calculated from MD simulations and theory, respectively.

Conclusions

The ice–liquid–ice transition reported in this paper confirms that the processes of electromelting and electrofreezing can occur in one system. The mechanism of this unexpected phenomenon is the surface charge induced change of the orientations of water dipoles, which leads to the change of the water–water interactions from being attractive to repulsive at a critical charge value q_c. Below q_c, the strength of the attractive water–water interactions decreases with increasing q, which induces electromelting. Above q_c, the strength of the repulsive water–water interactions increases with increasing q, which induces electrofreezing. Our results not only expand our knowledge of the graphene–water interface, but related analyses also uncover the mechanisms of electromelting and electrofreezing.

Acknowledgements

This work was jointly supported by the National Natural Science Foundation of China (NSFC, grant no. 11372313 and 11202213), the Key Research Program of the Chinese Academy of Sciences (grant no. KJZD-EW-M01), and the Instrument Developing Project of the Chinese Academy of Sciences (grant no. Y2010031).

Notes and references

1 P. A. Thiel and T. E. Madey, *Surf. Sci. Rep.*, 1987, **7**, 211–385.
2 M. A. Henderson, *Surf. Sci. Rep.*, 2002, **46**, 1–308.
3 A. Hodgson and S. Haq, *Surf. Sci. Rep.*, 2009, **64**, 381–451.
4 O. Teschke, *Langmuir*, 2010, **26**, 16986–16990.
5 K. B. Jinesh and J. W. M. Frenken, *Phys. Rev. Lett.*, 2008, **101**, 036101.
6 E. Bonaccurso, M. Kappl and H. J. Butt, *Curr. Opin. Colloid Interface Sci.*, 2008, **13**, 107–119.
7 N. Patra, B. Y. Wang and P. Kral, *Nano Lett.*, 2009, **9**, 3766–3771.
8 R. R. Nair, H. A. Wu, P. N. Jayaram, I. V. Grigorieva and A. K. Geim, *Science*, 2012, **335**, 442–444.
9 X. F. Feng, S. Maier and M. Salmeron, *J. Am. Chem. Soc.*, 2012, **134**, 5662–5668.
10 C. H. Y. X. Lim, A. Sorkin, Q. L. Bao, A. Li, K. Zhang, M. Nesladek and K. P. Loh, *Nat. Commun.*, 2013, **4**, 1556.
11 H. Li and X. C. Zeng, *ACS Nano*, 2012, **6**, 2401–2409.
12 R. Zangi and A. E. Mark, *Phys. Rev. Lett.*, 2003, **91**, 025502.
13 N. Giovambattista, P. J. Rossky and P. G. Debenedetti, *Phys. Rev. Lett.*, 2009, **102**, 050603.
14 S. H. Han, M. Y. Choi, P. Kumar and H. E. Stanley, *Nat. Phys.*, 2010, **6**, 685–689.
15 J. Cheh, Y. Gao, C. L. Wang, H. Zhao and H. P. Fang, *J. Stat. Mech.: Theory Exp.*, 2013, **6**, P06009.
16 C. Q. Zhu, H. Li, Y. F. Huang, X. C. Zeng and S. Meng, *Phys. Rev. Lett.*, 2013, **110**, 126101.
17 W. P. Lv and R. A. Wu, *Nanoscale*, 2013, **5**, 2765–2775.
18 X. F. Xia and M. L. Berkowitz, *Phys. Rev. Lett.*, 1995, **74**, 3193–3196.
19 I. M. Svishchev and P. G. Kusalik, *J. Am. Chem. Soc.*, 1996, **118**, 649–654.
20 I. Braslavsky and S. G. Lipson, *Appl. Phys. Lett.*, 1998, **72**, 264–266.
21 R. Zangi and A. E. Mark, *J. Chem. Phys.*, 2004, **120**, 7123–7130.
22 E. M. Choi, Y. H. Yoon, S. Lee and H. Kang, *Phys. Rev. Lett.*, 2005, **95**, 085701.
23 H. Qiu and W. L. Guo, *Phys. Rev. Lett.*, 2013, **110**, 195701.
24 S. Plimpton, *J. Comput. Phys.*, 1995, **117**, 1–19.
25 X. Y. Zhu, Q. Z. Yuan and Y. P. Zhao, *Sci. Rep.*, 2012, **2**, 927.
26 H. J. C. Berendsen, J. R. Grigera and T. P. Straatsma, *J. Phys. Chem.*, 1987, **91**, 6269–6271.
27 E. Sanz, C. Vega, J. L. F. Abascal and L. G. MacDowell, *Phys. Rev. Lett.*, 2004, **92**, 255701.
28 M. W. Mahoney and W. L. Jorgensen, *J. Chem. Phys.*, 2000, **112**, 8910–8922.
29 M. W. Mahoney and W. L. Jorgensen, *J. Chem. Phys.*, 2001, **114**, 363–366.
30 C. Vega and E. de Miguel, *J. Chem. Phys.*, 2007, **126**, 154707.
31 M. A. Gonzalez and J. L. F. Abascal, *J. Chem. Phys.*, 2010, **132**, 096101.
32 F. Cunha and N. J. Tao, *Phys. Rev. Lett.*, 1995, **75**, 2376–2379.
33 J. M. Campanera, G. Savini, I. Suarez-Martinez and M. I. Heggie, *Phys. Rev. B: Condens. Matter Mater. Phys.*, 2007, **75**, 235449.
34 K. Hermann, *J. Phys.: Condens. Matter*, 2012, **24**, 314210.
35 R. Balog, B. Jorgensen, L. Nilsson, M. Andersen, E. Rienks, M. Bianchi, M. Fanetti, E. Laegsgaard, A. Baraldi, S. Lizzit, Z. Sljivancanin, F. Besenbacher, B. Hammer, T. G. Pedersen, P. Hofmann and L. Hornekaer, *Nat. Mater.*, 2010, **9**, 315–319.
36 D. L. Miller, K. D. Kubista, G. M. Rutter, M. Ruan, W. A. de Heer, P. N. First and J. A. Stroscio, *Phys. Rev. B: Condens. Matter Mater. Phys.*, 2010, **81**, 125427.
37 S. Gladstone, K. Laidler and H. Eyring, *The theory of rate processes*, McGraw-Hill Book Company, Princeton University, New York, 1941.
38 L. D. Landau and E. M. Lifshitz, *Theory of Elasticity*, Butterworth-Heinemann, Oxford, 3rd edn, 1986.